ACS OMEGA

http://pubs.acs.org/journal/acsodf

Article

Identification of Bioactive SNM1A Inhibitors

Beverlee Buzon,[#] Ryan A. Grainger,[#] Cameron Rzadki, Simon York Ming Huang, and Murray Junop*

Cite This: *ACS Omega* 2021, 6, 9352−9361

Read Online

ACCESS | Metrics & More | Article Recommendations | Supporting Information

ABSTRACT: SNM1A is a nuclease required to repair DNA interstrand cross-links (ICLs) caused by some anticancer compounds, including cisplatin. Unlike other nucleases involved in ICL repair, SNM1A is not needed to restore other forms of DNA damage. As such, SNM1A is an attractive target for selectively increasing the efficacy of ICL-based chemotherapy. Using a fluorescence-based exonuclease assay, we screened a bioactive library of compounds for inhibition of SNM1A. Of the 52 compounds initially identified as hits, 22 compounds showed dose−response inhibition of SNM1A. An orthogonal gel-based assay further confirmed nine small molecules as SNM1A nuclease activity inhibitors with IC_{50} values in the mid-nanomolar to low micromolar range. Finally, three compounds showed no toxicity at concentrations able to significantly potentiate the cytotoxicity of cisplatin. These compounds represent potential leads for further optimization to sensitize cells toward chemotherapeutic agents inducing ICL damage.

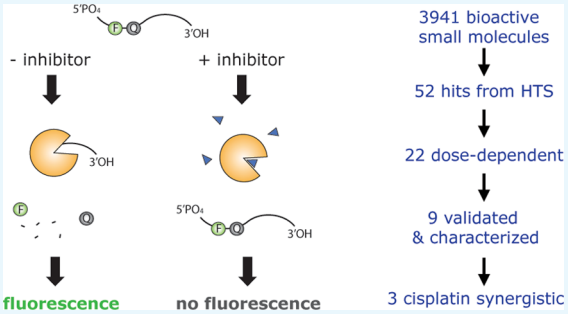

INTRODUCTION

Interstrand cross-links (ICLs) are a type of DNA damage in which opposing strands of DNA are covalently joined. ICL lesions are highly cytotoxic since they inhibit strand separation required for DNA replication and transcription.[1] This cytotoxicity has been successfully exploited in anticancer therapies for a broad range of tumors.[2] Cisplatin, a platinum-based ICL-inducing compound, is among the first-line drugs in treating solid mass malignancies, especially effective against ovarian and testicular cancers.[3] Despite initial therapeutic success in response to cisplatin-based chemotherapy, toxicity limits the full therapeutic dosing of cisplatin, which frequently leads to the generation of refractory tumors.[4] Development of acquired drug-resistant tumors results in high therapeutic failure rates and cancer relapse.[4] Acquired platinum resistance is partially mediated by increased DNA repair of ICL lesions, as evidenced by correlations in the DNA repair factor expression and therapeutic response to cisplatin.[5,6] Inhibition of ICL repair, therefore, has the promise of augmenting anticancer therapies.

Unlike most forms of DNA damage, which are simply repaired by damage excision and strand ligation, ICLs are particularly problematic to the cell since both strands of DNA are damaged. Therefore, to tackle the complexity of ICL removal, repair proteins from pathways dedicated to several types of DNA damages are employed.[7] The critical step that commits the cell to ICL repair is unhooking, in which structure-specific endonuclease XPF-ERCC1 makes the initial strand incision.[8] Given the central role of XPF-ERCC1 in ICL repair as well as the clinical correlations of ERCC1 in chemotherapeutic outcomes, efforts have focused on developing XPF-ERCC1 inhibitors to combat resistance to ICL-inducing agents.[5,6,9,10] Unfortunately, XPF-ERCC1 inhibitors lack ICL repair specificity due to the absolute requirement of XPF-ERCC1 in nucleotide excision repair (NER).[11,12] Other possible ICL nuclease targets include MUS81-EME1, SLX1-SLX4, FAN1, and SNM1B, but their moderated hypersensitivity compared to XPF-ERCC1 suggests roles either less crucial or downstream in the repair pathway.[13] Additional functions of these nucleases in replication fork maintenance and repair make them less ideal candidates for ICL sensitization efforts.[14−16]

SNM1A nuclease has been shown to be involved in ICL but no other DNA repair pathways. Cells in which SNM1A is depleted or inactivated result in hypersensitivity to ICL-inducing agents.[17−19] Human SNM1A has also been implicated in cancer risk and prognosis.[20,21] SNM1A is epistatic with XPF-ERCC1, showing similar hypersensitivity defects in response to ICL-inducing agents in human cells, suggesting that both may be involved in unhooking.[19] SNM1A has 5′−3′ 5′ phosphate-dependent exonuclease activity and structure-specific endonuclease activity.[22,23] It is uncertain at what point SNM1A uses these activities, particularly during the unhooking process. While the precise function of SNM1A in ICL repair is unclear, the fact that catalytically active SNM1A

Received: July 23, 2020
Accepted: March 2, 2021
Published: March 31, 2021

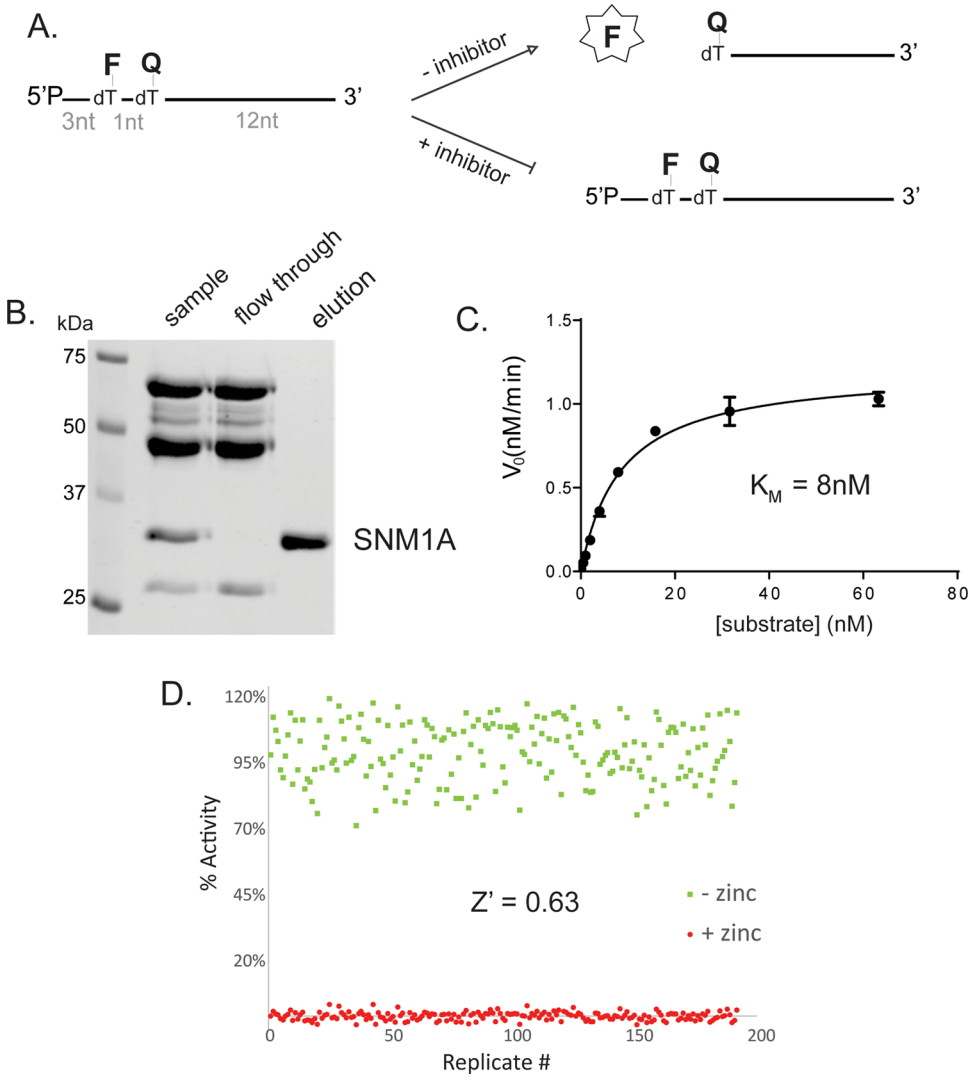

Figure 1. HTS assay for SNM1A inhibitors. (A) Schematic of the HTS oligonucleotide substrate (5P-FQ listed in Figure S1) with a fluorophore−quencher pair and expected products with or without an inhibitor. (B) Purified SNM1A after final cation exchange chromatography. The SNM1A-containing sample was immobilized to S-Seph (GE Healthcare) at 300 mM and eluted with a linear salt gradient (0.3−1 M). Eluted SNM1A-containing fractions were pooled and concentrated. Fractions were resolved with 12% SDS-PAGE containing trichloroethanol. Gel was visualized using stain-free enabled GelDoc (Bio-Rad). (C) K_M determination of purified SNM1A and 5P-FQ. Fluorescence was measured every minute for 2 h at 26 °C at 526 nm using the BioTek Synergy 4 Hybrid microplate reader. The assay was performed in triplicate, and K_M was determined using GraphPad Prism. (D) Z' score determination for the HTS SNM1A inhibition assay. SNM1A (3 nM) was incubated with 8 nM HTS substrate with and without zinc control for 40 min. Fluorescence was measured with an EnVision plate reader (PerkinElmer) at 535 nm.

is needed for repair makes SNM1A an ideal target for inhibition to specifically sensitize cells to ICL-inducing agents.[24,25]

The development of SNM1A inhibitors has gained significant interest, particularly since an epistatic relationship between SNM1A and XPF-ERCC1 was established.[19] Although compounds that inhibit SNM1A in vitro have been identified, there are no SNM1A inhibitors demonstrating cellular effects.[26−28] Screening biologically active small molecules for SNM1A inhibition may therefore be a promising strategy for ICL sensitization.

Here, we report the identification of small molecules from an HTS library of bioactive compounds that inhibit SNM1A. Initial hits were validated and further characterized for inhibition of SNM1A exonuclease and endonuclease activities. Finally, SNM1A inhibitors were tested in cells to assess enhanced cell killing in the presence of cisplatin. Three small molecules were identified that not only inhibit SNM1A activity in vitro but also sensitize cells toward ICL damage and therefore have the potential to prevent the repair of ICLs generated during ICL-based chemotherapy treatment.

RESULTS

High-Throughput Screening for SNM1A Inhibitors. To identify compounds that inhibit SNM1A nuclease activity, we utilized a fluorescence-based assay monitoring SNM1A exonuclease activity.[23] In this assay, a single-strand DNA substrate containing 5′ phosphate and an internal fluorophore−quencher pair (fluorescein−black hole quencher 1) results in attenuated fluorescence when nuclease activity is inhibited (Figure 1A). The assay was performed with purified recombinant SNM1A$^{698-1040}$ (Figure 1B), encompassing the active nuclease domain and the DNA substrate at the determined K_M (Figure 1C) such that both competitive and

https://doi.org/10.1021/acsomega.0c03528
ACS Omega 2021, 6, 9352−9361

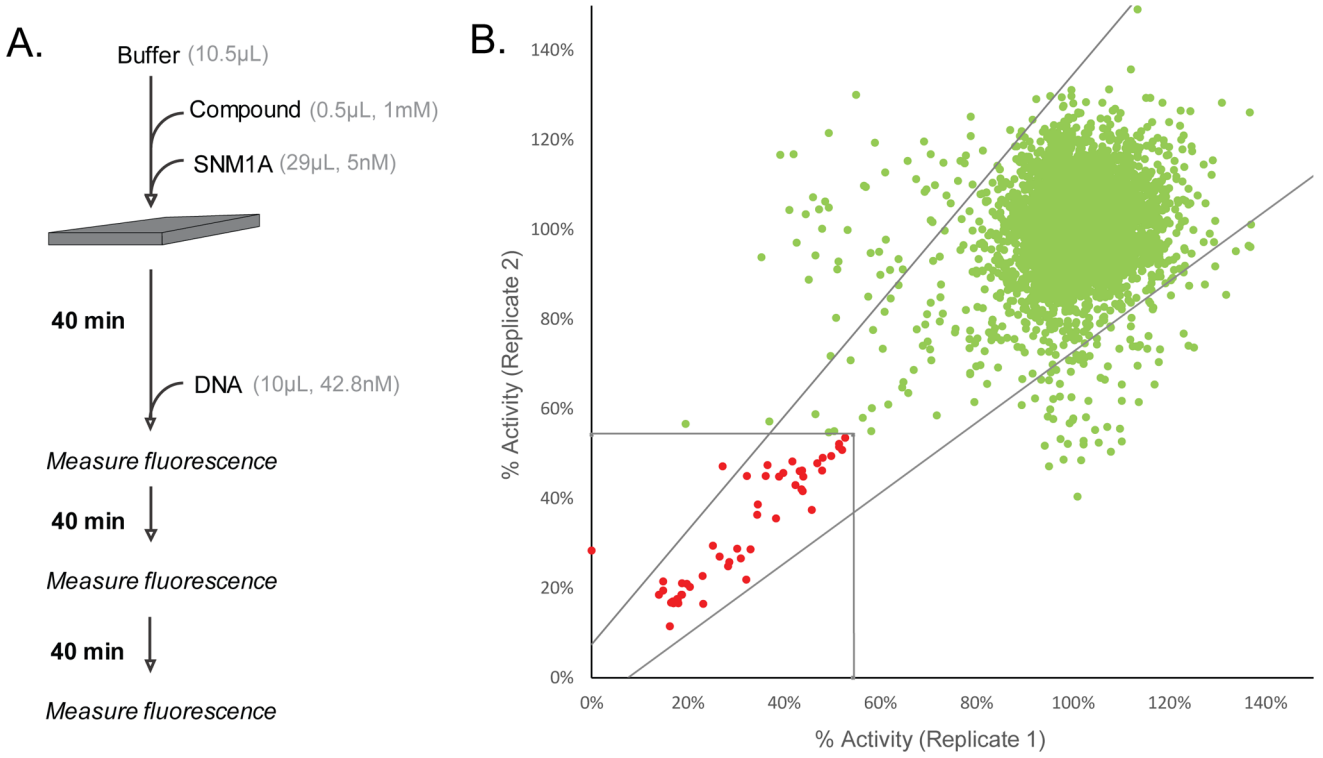

Figure 2. Putative HTS hits of SNM1A inhibitors. (A) Schematic of the HTS assay. (B) Replica plot of the HTS campaign of 3941 compounds. Percent activity was calculated as the difference between readings after 80 and 0 min. Diagonal lines indicate standard deviation of high controls. Boxed area indicates assay cutoff for possible inhibitors. Red dots indicate HTS assay hits and potential SNM1A inhibitors. Green dots indicate compounds that do not meet the cutoff and do not inhibit SNM1A.

noncompetitive inhibitors could be detected. Further assay development included modifications to fluorophore−quencher pair positioning and buffer composition to increase the specificity and signal. Zinc acetate was previously shown to inhibit SNM1A and was therefore used as the inhibited control for the assay.[23] The final assay demonstrated a Z' score of 0.63 (Figure 1D), indicating an acceptable detection window for identifying inhibitors by high-throughput screening.

Primary HTS Screen of Bioactive Library. We narrowed our screening campaign scope to a curated library of 3941 bioactive compounds composed of natural products, off-patent FDA-approved drugs, and drug-like synthetic small molecules. Limiting screening to the bioactive library was anticipated to improve the success of downstream cell-based inhibitor characterization. Using the assay protocol in Figure 2A, 3941 small molecules on 26 separate plates were screened for SNM1A inhibition in duplicate. Final HTS fluorescence values after 80 min of incubations for each compound were normalized with respect to high (uninhibited) and low (inhibited) controls on each plate to adjust the minimum and maximum signals. Control-based normalization permitted fluorescence comparison among plates, not just within individual plates. The interquartile mean (IQM) was also used for secondary normalization to limit the effect of outliers.[29] The high control-based hit rate cutoff was 54%, representing three standard deviations from the mean of uninhibited reactions (boxed area in Figure 2B). After both control-based and IQM-based normalization, the number of hits was reduced from 114 to 52 compounds (red dots in Figure 2B, listed in Figure S2).

Validation of HTS Hits by Dose−Response Analysis. A dose−response screen using the same protocol in Figure 2A was used to validate that identified compounds decreased fluorescence in the initial screen. This second screen was not only to confirm that the compound of interest reproducibly showed inhibition but also to eliminate false positives due to the plate position. Inhibitors were tested for a dose-dependent response using concentrations in the low nanomolar to mid-micromolar range. Of the 52 compounds tested (Figure S3), 22 showed reasonable dose-dependent inhibition (Figure 3A) and were selected for further confirmation by a secondary gel-based assay.

Secondary Gel-Based Validation and Characterization. Although the HTS assay was robust and reproducible, it was necessary to perform an orthogonal nuclease assay given the intrinsic fluorescence of many compounds in the bioactive library. A gel-based exonuclease activity assay utilizing a single-strand DNA substrate (5P-3F) containing a 5′ phosphate and 3′ fluorophore was used to validate inhibition of SNM1A (Figure 3B). Since SNM1A is a nonprocessive 5′ exonuclease, inhibitor validation was carried out by monitoring shortened products in response to two compound concentrations (25 and 6.25 μM). In this semiquantitative assay, compounds whose products were smaller than 15 nucleotides (or more than 50% digested) did not show sufficient inhibition to warrant further investigation (in red). Note that compounds **44** and **54** (indicated with †) were also excluded due to internal fluorescence. Nine of 22 compounds (in black) demonstrated >50% inhibition of SNM1A by the gel-based assay and were carried forward for further characterization.

To further analyze the kinetics of SNM1A exonuclease inhibition, a substrate with a 5′ phosphate and an internal fluorophore at the first nucleobase (listed in Figure S1 as 5P-1F) was used to enable the visualization of a single exonuclease

https://doi.org/10.1021/acsomega.0c03528
ACS Omega 2021, 6, 9352−9361

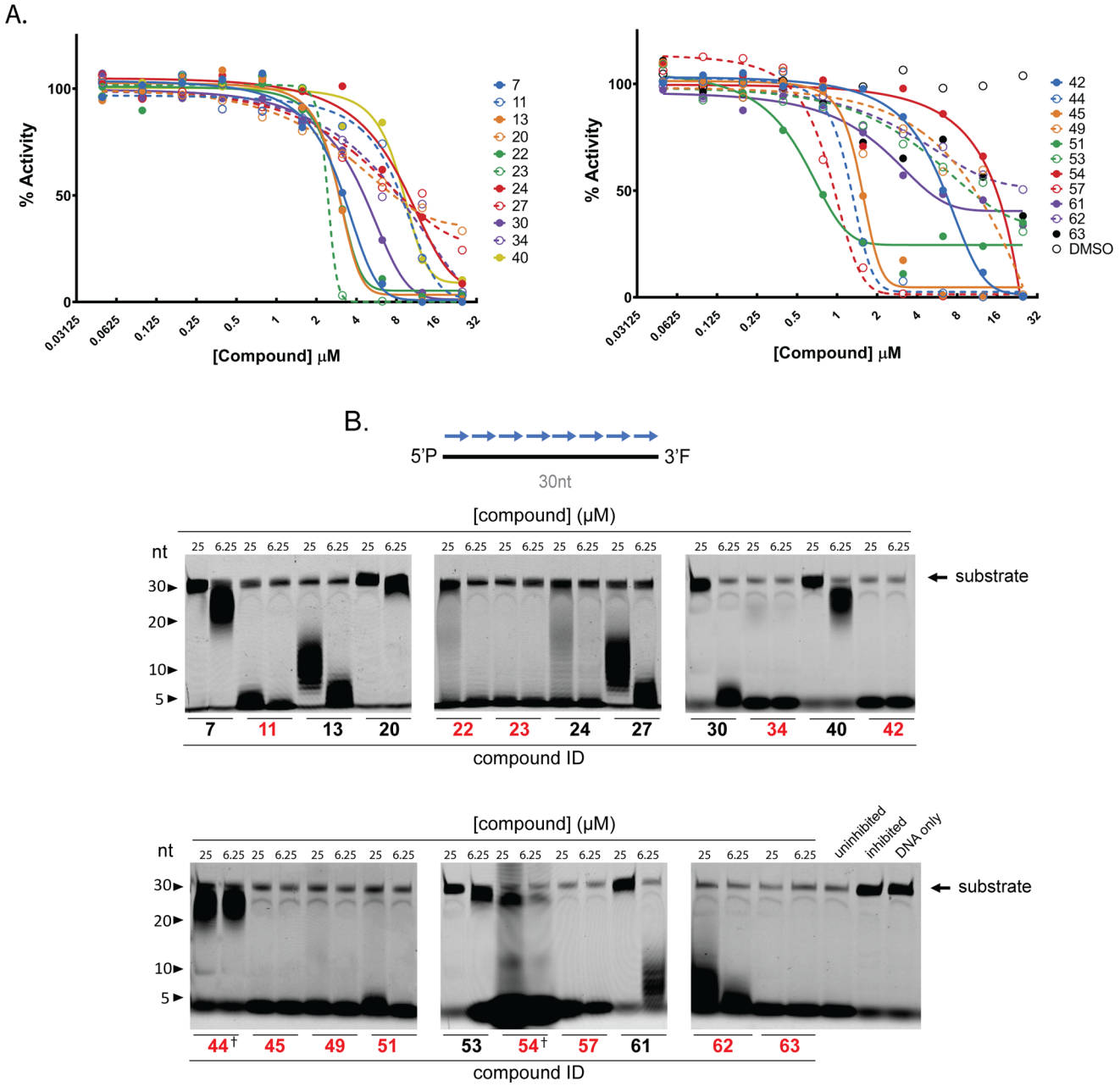

Figure 3. Validation of SNM1A inhibitors. (A) HTS hit validation with dose-dependent inhibition screen. Hits from Figure 2B were tested for dose−response inhibition in duplicate. Only compounds exhibiting dose−response inhibition in at least the low micromolar range are shown. All other curves are shown in Figure S3. (B) Gel-based secondary screen of putative SNM1A inhibitors. SNM1A (3 nM) was assayed with 25 and 6.25 μM compound, as noted. Inhibited and uninhibited reactions utilized zinc acetate (1 mM) and DMSO, respectively. A single-stranded 30mer oligonucleotide substrate (50 nM) containing a 3′ fluorophore is shown and listed in Figure S1 as 5P-3F. Products from nonprocessive exonuclease activity of SNM1A result in a shortening of the substrate. Products were resolved using 20% denaturing PAGE and imaged with the Typhoon imager (GE Healthcare) at 526 nm. Compounds in red were excluded from further characterization. The dagger symbol refers to compounds exhibiting intrinsic internal fluorescence.

event (shown in Figure 4A). Similarly, characterization of SNM1A endonuclease inhibition was carried out using a gapped substrate containing a 5′ fluorophore (5F-gap) that permitted observation of a single cleavage product (Figure 4B). The compound concentration required to inhibit half the nuclease activity (or IC_{50}) of SNM1A was determined for each compound (Figures S4 and S5). A comparison of IC_{50} values for exonuclease and endonuclease inhibitions is presented in Figure 4C. Compounds **40**, **20**, and **53** were the most potent exonuclease activity inhibitors, acting in the nanomolar range. Compounds **40**, **20**, and **30** also appeared to preferentially inhibit exonuclease activity since more than a 10-fold increase in inhibitor concentration was required to inhibit endonuclease activity to similar levels.

Cisplatin Potentiation Assay. We hypothesized that these bioactive SNM1A inhibitors may enhance the toxicity of ICL-inducing agents, specifically of cisplatin. Cisplatin sensitization was tested in HeLa cells by monitoring cell survival in the absence or presence of SNM1A inhibitors and cisplatin (Figure 5A). Although the in vitro IC_{50} value was

https://doi.org/10.1021/acsomega.0c03528
ACS Omega 2021, 6, 9352−9361

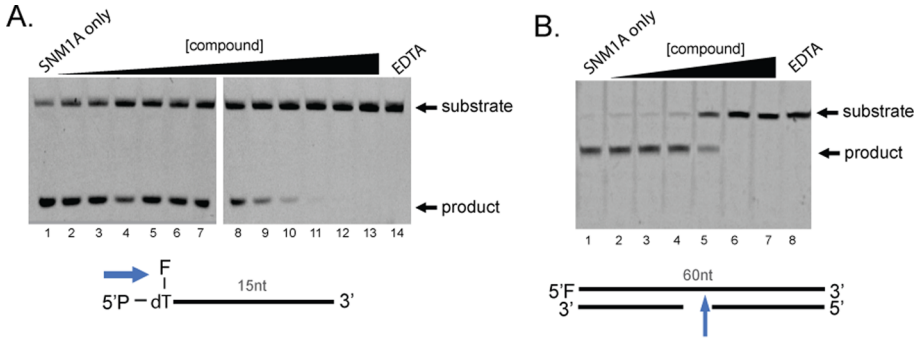

C.

SNM1A Inhibitor	Exonuclease IC_{50} (μM)	SEM	Endonuclease IC_{50} (μM)	SEM	Fold difference of endo/exo
40	0.08	0.01	1.9	0.25	25
20	0.12	0.01	1.6	0.31	13
53	0.36	0.10	2.1	1.1	6.0
30	1.7	0.21	22	2.0	13
61	2.8	1.4	indeterminate	-	-
24	12	2.3	31	1.2	2.5
27	35	1.5	25	6.8	0.7
13	38	11	27	5.7	0.7
7	68	13	195	31	2.9

Figure 4. Gel-based dose–response assays for IC_{50} determination. (A) Representative results for the gel-based assay for exonuclease IC_{50} determination. Schematic of the single-strand exonuclease substrate (5P-1F in Figure S1) is shown. The product is a single 5′ nucleotide with a fluorophore. Lanes 2–13 represent reactions with an inhibitor, increasing 2-fold per lane. Each assay was designed such that the IC_{50} values lay between lanes 6 and 9. (B) Representative gel for the gel-based assay for endonuclease IC_{50} determination. Gapped endonuclease substrate schematic is shown (5F-gap in Figure S1). The product is a 35mer oligonucleotide with a 5′ fluorophore. Lanes 2–7 represent reactions with a compound, increasing 4-fold per lane. Each assay was designed such that the IC_{50} values lay between lanes 3 and 5. SNM1A (0.2 nM, 200 nM) was incubated with a substrate (110 nM, 30 nM) for 60 or 150 min for exonuclease and endonuclease inhibitions, respectively. Products were resolved using 23% denaturing PAGE and imaged with the ChemiDoc at 526 nm. Products were quantified with ImageLab (Bio-Rad). All assays were performed in triplicate. (C) Summary of IC_{50} values of SNM1A exonuclease and endonuclease activities. IC_{50} was determined using GraphPad Prism. F denotes the fluorophore, P denotes the phosphorylation, and SEM denotes the standard error of the mean.

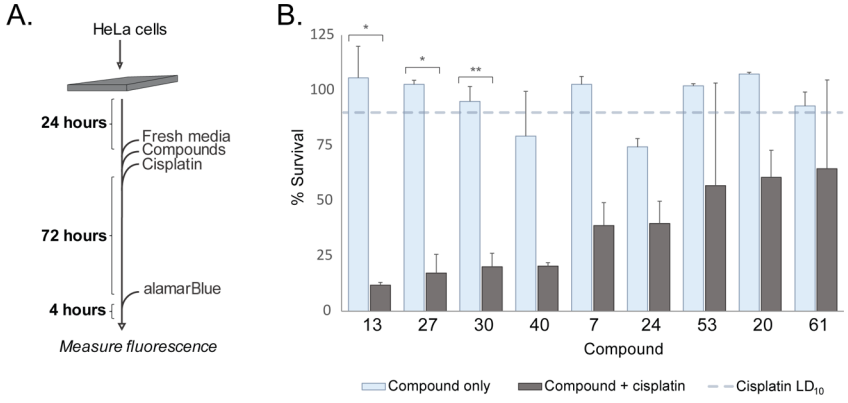

Figure 5. SNM1A inhibitors potentiate cisplatin toxicity. (A) Schematic of the cisplatin potentiation assay. (B) Cisplatin potentiation with SNM1A inhibitors (25 μM). Cell survival is reported for the LD_{10} value of cisplatin (dashed line) as well as with cisplatin (LD_{10}, 15 μM, in dark gray) or without (light blue). Relative % survival is expressed as percent normalized to cells incubated with control vehicle (DSMO) only. Assays were performed in duplicate, where error bars represent SEM. One asterisk symbol denotes a *t* test significance of $p < 0.05$, and two asterisk symbols denote $p < 0.01$ of inhibitor alone vs inhibitor and cisplatin.

determined, cells were exposed to the highest concentration of the compound (25 μM) since it was unclear how the compounds would behave in the cell. Compounds were tested with or without a sublethal dose of cisplatin (LD_{10}, dashed line, 15 μM). Of the nine inhibitors of SNM1A, only compound **24** itself demonstrated inherent toxicity at 25 μM. In contrast, all other compounds had little to no effect on cell viability on their own (Figure 5B, light blue bars). With sublethal concentrations of cisplatin, however, three compounds (**13**, **27**, and **30**) showed reduced cell survival (Figure 5B, dark gray bars) and cytotoxicity was significantly augmented. The observed synergy is important, as it indicates that while the

https://doi.org/10.1021/acsomega.0c03528
ACS Omega 2021, 6, 9352–9361

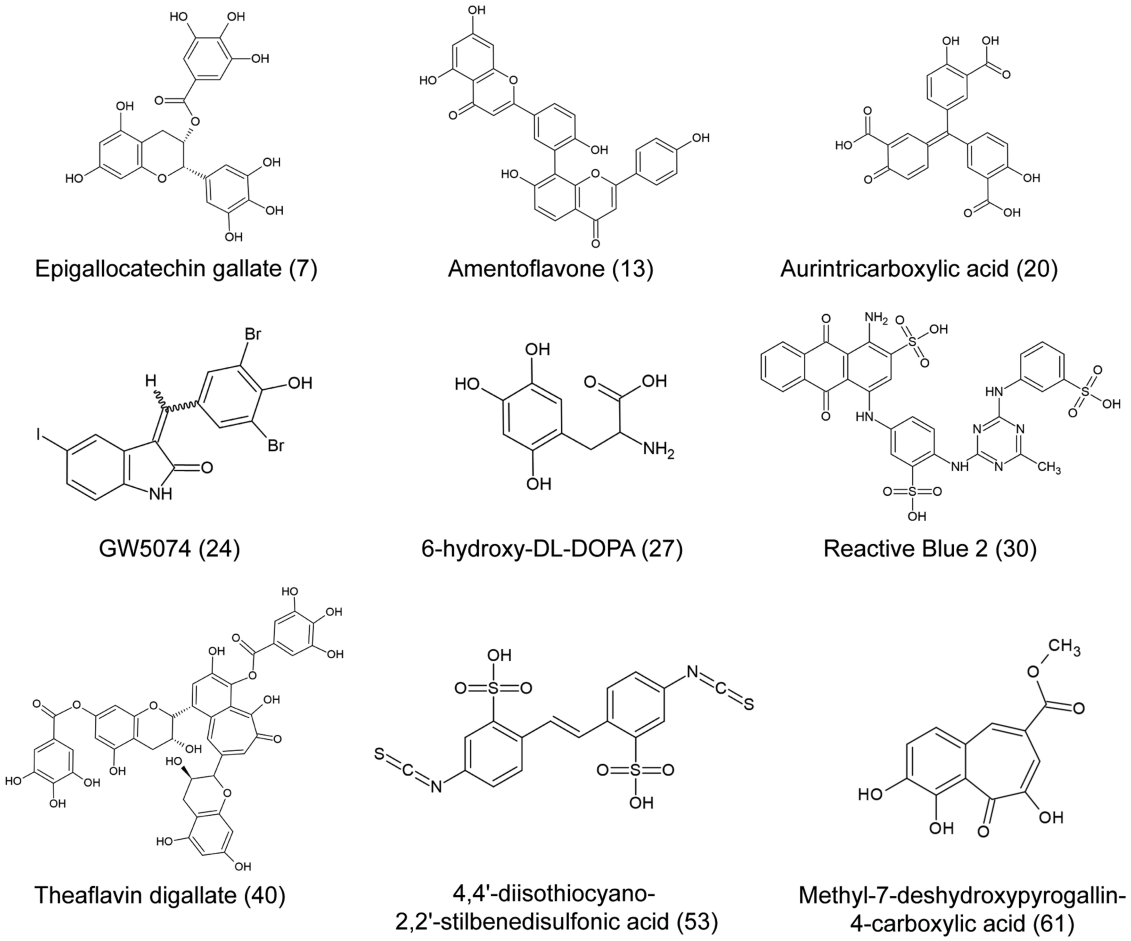

Figure 6. Inhibitors of SNM1A.

identified SNM1A inhibitors themselves are nontoxic to the cell, they appreciably potentiate the toxicity of cisplatin.

DISCUSSION

Chemotoxicity and chemoresistance render cancer management a complicated and challenging process; however, DNA repair inhibition has been an effective anticancer strategy in the clinic.[30] Restricting repair of DNA damage has been shown to improve the therapeutic efficacy of DNA damage-based chemotherapies, best exemplified by the development of PARP inhibitors in breast cancer treatment.[31] However, ensuring that the appropriate repair pathway is blocked for chemotherapeutic, but not endogenous, damage can be tricky.[32] This is particularly difficult with ICL-based agents since ICL repair uses proteins from several pathways required for repair of other types of damages (i.e., reactive oxygen species and UV radiation).[33] Unlike other ICL repair factors that play additional roles in DNA repair (i.e., XPF-ERCC1), SNM1A is exclusively involved in the repair of ICL-induced lesions in human cells. As such, SNM1A is an attractive target for inhibition of ICL repair, thereby sensitizing tumors to ICL-based chemotherapy, although simultaneously targeting NER and ICL may also be effective. Focused efforts on the development of SNM1A inhibitors are further strengthened with recent reports, demonstrating ICL sensitivity in H1299 carcinoma cells with the loss of SNM1A.[17]

Efforts have focused on inhibiting the SNM1A nuclease domain (metallo-β-lactamase fold), which hydrolyzes an array of substrates, including β-lactams.[27] A previous study screening a panel of β-lactam compounds identified several cephalosporins able to inhibit SNM1A.[27] Despite considerable in vitro inhibition, they lacked sufficient membrane permeability to be functional at the cellular level.[27] More recently, targeted inhibition of the SNM1A catalytic site has yielded compounds that demonstrate modest inhibition, but these have not yet been tested in cells.[26,28] We chose to conduct screening for SNM1A inhibitors using a library of bioactive compounds biased toward cell permeability. Hits identified from our screen of bioactive compounds not only demonstrated inhibition of SNM1A nuclease activities in vitro but also increased cisplatin sensitivity in cells when administered concurrently with cisplatin.

It is plausible that some SNM1A inhibitors identified in this study (Figure 6) may act nonspecifically on nucleases, resulting in hypersensitivity to cisplatin damage. To test the possibility that inhibition resulted from nonspecific interactions between the inhibitor and DNA, we measured the displacement of the DNA-binding compound, ethidium bromide, from a short duplex DNA substrate (EtBr-DS in Figure S1). While compounds **7**, **13**, **24**, **53**, and **61** do not appear to significantly displace ethidium bromide in Figure S6, compounds **20**, **27**, **30**, and **40** have apparent nonspecific interactions with DNA, suggesting that this effect may contribute to their mechanism of SNM1A inhibition. Consistent with this interpretation, compound **20** is known to function as a nonspecific nuclease inhibitor.[34] Finally, compounds **7**, **27**, **40**, and **61** contain a

https://doi.org/10.1021/acsomega.0c03528
ACS Omega 2021, 6, 9352−9361

catechol moiety, which may bind metal within the active site of SNM1A and possibly other metal-dependent enzymes.[35] It is unlikely that the mechanism of inhibition is based on the nonspecific interaction of catechols with active site metals since the initial bioactive library contained 166 molecules with catechol moieties that were not identified as inhibitors.

Follow-up studies evaluating these compounds in an SNM1A knockout or knockdown in cells will be required to evaluate specificity for SNM1A. These crucial experiments may be challenging because SNM1A homologs, SNM1B (also involved in ICL repair) and SNM1C, share a similar active site. In support of the cross-inhibition of SNM1A homologs, we tested the SNM1A inhibitors against the nuclease domain for SNM1B (Figure S7). While some compounds were found to be specific to SNM1A, several decreased exonuclease activity of SNM1A and SNM1B equally. Inhibition of both SNM1A and SNM1B activities may be a beneficial strategy since they participate in distinct steps of ICL repair, but the results from Figure S7 underscore the necessity of careful assessment of these inhibitors in the cell.

The specificity of these compounds for SNM1A over the homologs or other nucleases can be improved using structure−activity relationship studies. Determining inhibitor-bound structures of SNM1A will also be beneficial for elucidating the mechanism(s) of inhibition. Structure−function studies will be particularly important for inhibitors that differentially inhibit SNM1A exonuclease and endonuclease activities. Currently, it is not clear how distinct SNM1A nuclease activities promote ICL repair. Because SNM1A uses the same active site for all nuclease activities, it may not be possible to generate separation of function mutations. Developing selective inhibitors toward each nuclease activity may help to dissect their precise roles in ICL repair.

Cisplatin is a widely used first-line chemotherapeutic for the treatment of a broad range of cancers. However, chemoresistance is a clinically significant problem that restricts the use of cisplatin and other platinum-based agents. Here, we have identified and characterized bioactive compounds that inhibit SNM1A and augment cisplatin sensitivity. Given the importance of cisplatin as an anticancer agent, identification of adjuvant ICL repair inhibitors provides an opportunity to reduce nontargeted cisplatin-associated toxicity and increase its therapeutic effect in chemotherapy.

METHODS

Protein Expression and Purification. Human SNM1A (Uniprot: Q6PJP8) was truncated to the nuclease domain encompassed by residues 698−1040. Recombinant SNM1A was expressed in Star pRARE pLysS *Escherichia coli* (Invitrogen) and induced at 0.700 OD_{600} with 1 mM IPTG at 25 °C overnight. Cells were resuspended in nickel A buffer (50 mM Tris (pH 7.5), 500 mM NaCl, 30 mM imidazole, 0.5 mM TCEP, 0.01% Triton X-100, and 10% glycerol) and protease inhibitors (3 μM aprotinin, 1 μM pepstatin A, 1 mM benzamidine, 1 μM leupeptin, and 1 mM PMSF) and then lysed with three passes through a cell disruptor at 10,000 psi. The lysate was clarified by centrifugation at 48,000*g* for 40 min and filtered. The sample was loaded onto a HisTrap HP nickel-chelating column (GE Healthcare) and step eluted with nickel A buffer containing 210 mM imidazole. The sample was diluted to 300 mM NaCl using QA buffer (50 mM Tris (pH 8.5), 0.5 mM TCEP, and 10% glycerol) and loaded onto a Q Sepharose HP column (GE Healthcare). Protein was then eluted with 400 mM NaCl. TEV protease was added at 5:1 SNM1A to TEV to cleave the His_6-NusA fusion protein overnight. The cleaved sample was diluted with SA buffer (50 mM Tris (pH 7.5), 0.5 mM TCEP, and 10% glycerol) to 300 mM NaCl before loading onto an SP HP Sepharose column (GE Healthcare). Protein was eluted with a linear gradient from 300 mM to 1 M NaCl. SNM1A-containing fractions were pooled and concentrated with a 10 kDa MWCO Centricon (Corning). Samples were flash frozen in liquid nitrogen and stored at −80 °C.

HTS Assay for SNM1A Inhibition. SNM1A nuclease reactions were performed in buffer containing 50 mM [tris(hydroxymethyl)methylamino]propanesulfonic acid (TAPS) buffer (pH 9.1), 10 mM magnesium acetate, 75 mM potassium acetate, 1 mM DTT, and 100 μg/mL bovine serum albumin. Reactions containing 3 nM SNM1A and 8 nM HTS substrate 5P-FQ were prepared in black, flat-bottom 384-well plates. Reactions were initiated with the addition of DNA substrate 5P-FQ. Fluorescence was measured using the BioTek Synergy 4 Hybrid microplate reader at 526 nm or EnVision plate reader (PerkinElmer) at 535 nm.

K_M Determination for SNM1A HTS Substrate. Reactions containing 25 nM SNM1A and DNA ranging from 1.25 to 400 nM were prepared in black, flat-bottom 384-well plates (Corning) on ice. Reactions were initiated with the addition of 5P-FQ DNA. Fluorescence was measured every minute for 2 h at 26 °C at 526 nm using the BioTek Synergy 4 Hybrid microplate reader. The initial velocity for each curve was calculated and plotted against corresponding substrate concentrations. Product formation, expressed as % fluorescence using the equation below, was used to determine kinetic parameters using GraphPad Prism 6.0.

$$\%\text{fluorescence} = \text{fluorescence}_p - \text{fluorescence}_n$$

where subscript p represents the fluorescence of SNM1A products and subscript n represents the fluorescence of the negative control.

Z' Factor Determination for HTS Assay. Z' determination for the HTS assay for SNM1A inhibitors was performed using the Biomek FX workstation (Beckman Coulter) equipped with a BioRAPTR (Beckman Coulter) liquid dispensing system. Buffer (10 μL) was added to all wells of a black 384-well plate. Dissolved compounds in DMSO (0.5 μM) were dispensed into each well. Zinc acetate (0.5 μL; final concentration: 1 mM) or water was added to the wells. Buffer containing 5 nM SNM1A was added (29 μL). Reactions (total: 40 μL) were incubated for 40 min at 26 °C. DNA (10 μL, 42.8 nM) was dispensed, and fluorescence was immediately measured with the EnVision plate reader (PerkinElmer) at 535 nm. Final endpoint measurements were taken after 80 min. Relative fluorescence unit (RFU) measurements were used to generate the Z' factor as defined by the following equation

$$Z' = 1 - (3(\sigma_H + \sigma_L))/(|\mu_H - \mu_L|)$$

where σ represents the mean, μ represents the standard deviation, subscript H represents the high activity control, and subscript L represents the zinc-containing low control.

Compound Preparation for HTS Campaign. The McMaster bioactive set, compiled by the Center for Microbial Chemical Biology (sourced from Prestwick, Biomol, LOPEC, and MicroSource), was used for high-throughput screening.

https://doi.org/10.1021/acsomega.0c03528
ACS Omega 2021, 6, 9352−9361

Compound preparation was performed using the Biomek FX workstation (Beckman Coulter) equipped with a BioRAPTR (Beckman Coulter) liquid dispensing system. 96-well plates containing compounds dissolved in DMSO were dispensed in duplicate wells of black 384-well microplates containing buffer only. For pilot and primary screening, 0.5 μL of 1 mM compound in DMSO (1% DMSO, 10 μM final) was dispensed into 10 μL of buffer using long pin tools. For dose−response screen, compounds ranging from 2.4 to 2500 nM were dispensed as described above.

Primary Fluorescence-Based HTS Campaign. The primary HTS screen for SNM1A inhibitors was performed using a Biomek FX workstation (Beckman Coulter) equipped with a BioRAPTR (Beckman Coulter) liquid dispensing system. Buffer (10.5 μL) was added to all wells of a black 384-well plate. Compounds were dispensed as described above. Zinc acetate (0.5 μL; final concentration: 1 mM) or water was added to 36 wells to standardize plate-to-plate variation. Buffer (29 μL) containing 5 nM SNM1A was then added. Reactions (total: 40 μL) were incubated for 40 min at 26 °C to replicate incubation time of compounds with SNM1A. Addition of DNA (10 μL, 42.8 nM) was dispensed, and fluorescence was immediately measured with the EnVision plate reader (PerkinElmer) at 535 nm. Midpoint and endpoint of the reactions were measured after 40 and 80 min, respectively. The percent activity of SNM1A in response to each compound was calculated from the measured RFU using the equation

$$\%\text{activity} = (S - L)/(H - L) \times 100\%$$

where S represents the measured sample value. H and L represent the mean of the high and low activity control of each plate, respectively.

HTS data were order-ranked, and the mean of the two middle quartiles determines the interquartile mean (IQM) to normalize data.

$$\text{IQM normalization activity} = (S/\mu_{\text{iq}})$$

where S represents the measured sample value and μ_{iq} represents the mean (μ) of the interquartile (iq) data of the plate. HTS hits were defined as samples below the control-based cutoff of all controls in the HTS campaign.

$$\text{control} - \text{based cutoff} = 1 - 3\mu_{\text{H}}$$

where μ represents the standard deviation and subscript H represents the high activity control.

Gel-Based Secondary Screen Validation. SNM1A reactions containing 3 nM SNM1A and 1% DMSO-dissolved compound (6.25 and 25 μM final) were incubated at room temperature for 40 min. Reactions were initiated by addition of 50 nM DNA substrate, 5P-3F, incubated at 37 °C for 3 h. Reactions were stopped with the addition of formamide loading buffer (95% formamide, 10 mM EDTA). Products were separated using 20% denaturing PAGE and detected at 526 nm using the Typhoon imager (GE Healthcare).

Gel-Based Inhibitor Characterization. All reactions were performed at 37 °C in buffer containing 50 mM Tris-acetate (pH 7.2), 10 mM magnesium acetate, 75 mM potassium acetate, 1 mM DTT, and 100 μg/mL BSA. Unless indicated, exonuclease and endonuclease activities were measured with DNA substrate 5P-1F or 5F-gap, respectively. Reactions were stopped with the addition of formamide loading buffer. All gels were resolved with 23% denaturing PAGE and imaged with the ChemiDoc XRS (Bio-Rad) at 526 nm for 2 s.

Time Course Assay. To determine the concentration required for full substrate digestion at 60 min, 2 μM SNM1A was diluted 20- to 1200-fold, and a time course assay from 2 to 64 min was performed. A master mix containing diluted SNM1A was aliquoted and initiated with the addition of 100 nM DNA. Product formation, as a percentage of the total substrate, was calculated based on

$$\text{reaction progression} = (\%\text{product in reaction} - \%\text{product in control})/100$$

where a time point reflecting reaction progression of 20% was used for K_{M} determination.

K_{M} Determination. Reactions containing SNM1A (0.2 nM for exonuclease activity and 200 nM for endonuclease activity) were prewarmed for 2 min to 37 °C. DNA, ranging from 20 to 1000 nM, was added to initiate reactions after warming. Exonuclease reactions were incubated for 3 min and endonuclease reactions for 15 min. DNA was analyzed as described above. K_{M} reaction velocities were determined using

$$\text{velocity ([DNA]/s)} = (\text{reaction progression} \times [\text{DNA}])/(\text{time (s)})$$

Triplicate reaction velocities were curve-fitted using Michaelis−Menten kinetics on GraphPad Prism 6.0.

IC_{50} Determination. Reactions containing SNM1A (0.2 nM for exonuclease activity and 200 nM for endonuclease activity) and inhibitor in DMSO (30 nM to 250 μM) were incubated for 20 min at room temperature. DNA at K_{M} concentration (110 nM 5P-1F or 30 nM 5F-gap final) was added to initiate reactions. Exonuclease and endonuclease reactions proceeded at 37 °C for 60 or 150 min, respectively. Triplicate assays were curve-fitted using GraphPad Prism 6.0.

Cisplatin Dose−Response Assay. HeLa cells were seeded at 3500 cells/well in 96-well tissue culture-treated black plates in 100 μL of DMEM media. After 24 h, media were removed and replaced with fresh media containing 500 nM to 500 μM cisplatin. Untreated controls were included on all plates as a reference. Plates were incubated for 72 h before measuring cell viability using alamarBlue (Invitrogen), where 11 μL of alamarBlue was added directly to the media. Plates were then incubated at 37 °C in the dark for 3 h before fluorescence was measured at 590 nm. Lethal and sublethal cisplatin concentrations were derived from triplicate dose−response assays.

Cisplatin Potentiation Assay. HeLa cells were seeded at 3500 cells/well in 96-well tissue culture-treated black plates in 100 μL of DMEM media. After 24 h, media were removed and fresh media containing the compound(s) of interest were added (25 μM and 1% DMSO) ±15 μM cisplatin. Untreated controls were included on all plates as a reference. Plates were incubated for 72 h before measuring cell viability using alamarBlue (Invitrogen), where 11 μL of alamarBlue was added directly to the media. Plates were then incubated at 37 °C in the dark for 3 h before fluorescence was measured at 590 nm. Reported averages were derived from two independent experiments.

https://doi.org/10.1021/acsomega.0c03528
ACS Omega 2021, 6, 9352−9361

■ ASSOCIATED CONTENT

Supporting Information

The Supporting Information is available free of charge at https://pubs.acs.org/doi/10.1021/acsomega.0c03528.

List of oligonucleotides used in study; compound ID numbers; dose response and IC_{50} curves; ethidium bromide displacement of characterized inhibitors; SNM1B cross-inhibition of SNM1A inhibitors; and supplemental methods (PDF)

Accession Codes

SNM1A: Q6PJP8 and SNM1B: Q9H816.

■ AUTHOR INFORMATION

Corresponding Author

Murray Junop − *Department of Biochemistry and Biomedical Sciences, McMaster University, Hamilton, Ontario L8S 4L8, Canada; Department of Biochemistry, Western University, London, Ontario N6A 5C1, Canada;* orcid.org/0000-0001-6676-5717; Phone: 1 (519) 661-2017; Email: mjunop@uwo.ca; Fax: : 1 (519) 661-3175

Authors

Beverlee Buzon − *Department of Biochemistry and Biomedical Sciences, McMaster University, Hamilton, Ontario L8S 4L8, Canada; Department of Biochemistry, Western University, London, Ontario N6A 5C1, Canada;* orcid.org/0000-0002-2335-4448

Ryan A. Grainger − *Department of Biochemistry, Western University, London, Ontario N6A 5C1, Canada*

Cameron Rzadki − *Department of Biochemistry and Biomedical Sciences, McMaster University, Hamilton, Ontario L8S 4L8, Canada*

Simon York Ming Huang − *Department of Biochemistry and Biomedical Sciences, McMaster University, Hamilton, Ontario L8S 4L8, Canada*

Complete contact information is available at: https://pubs.acs.org/10.1021/acsomega.0c03528

Author Contributions

#B.B. and R.A.G. contributed equally to the completion of this paper. The manuscript was written by B.B., R.A.G., and M.J. All authors contributed to experimental design and data collection. All authors have approved the final version of the manuscript.

Funding

This study was funded by Canadian Institute of Health Research [MOP-89903] and Canadian Cancer Society [702157].

Notes

The authors declare no competing financial interest.

■ ACKNOWLEDGMENTS

A huge thanks to the McMaster Centre for Microbial Chemical Biology, particularly for Tracey Campbell's contributions for overseeing the HTS campaign, Fazmin Nizam for HTS data processing, and Cecilia Murphy and Jenny Wong for assisting with the screening. We thank Tracey and Susan McCusker for their work on the cell-based assays.

■ ABBREVIATIONS

HTS, high-throughput screening; ICL, interstrand cross-link; SNM1(A/B/C), sensitive to nitrogen mustard group 1 A/B/C; XPF, xeroderma pigmentosum group F; ERCC1, DNA excision repair cross-complementing group 1; FAN1, Fanconi anemia-associated nuclease 1; SLX(1/4), synthetic lethal of unknown genes 1/4; MUS81, methanesulfonate UV-sensitive protein 81; EME1, essential meiotic endonuclease 1; IQM, interquartile mean; PARP, poly-ADP ribose polymerase; NER, nucleotide excision repair

■ REFERENCES

(1) Noll, D. M.; Mason, T. M.; Miller, P. S. Formation and Repair of Interstrand Cross-links in DNA. *Chem. Rev.* **2006**, *106*, 277−301.

(2) Deans, A. J.; West, S. C. DNA Interstrand Crosslink Repair and Cancer. *Nat. Rev. Cancer* **2011**, *11*, 467−480.

(3) Florea, A.-M.; Büsselberg, D. Cisplatin as an Anti-Tumor Drug: Cellular Mechanisms of Activity, Drug Resistance and Induced Side Effects. *Cancers* **2011**, *3*, 1351−1371.

(4) Galluzzi, L.; Senovilla, L.; Vitale, I.; Michels, J.; Martins, I.; Kepp, O.; Castedo, M.; Kroemer, G. Molecular Mechanisms of Cisplatin Resistance. *Oncogene* **2012**, *31*, 1869−1883.

(5) Britten, R. A.; Liu, D.; Tessier, A.; Hutchison, M. J.; Murray, D. ERCC1 Expression as a Molecular Marker of Cisplatin Resistance in Human Cervical Tumor Cells. *Int. J. Cancer* **2000**, *89*, 453−457.

(6) Usanova, S.; Piée-Staffa, a.; Sied, U.; Thomale, J.; Schneider, a.; Kaina, B.; Köberle, B. Cisplatin Sensitivity of Testis Tumour Cells Is Due to Deficiency in Interstrand-Crosslink Repair and Low Ercc1-Xpf Expression. *Mol. Cancer* **2010**, *9*, 248.

(7) Dronkert, M. L. G.; Kanaar, R. Repair of DNA Interstrand Cross-Links. *Mutat. Res., DNA Repair* **2001**, *486*, 217−247.

(8) Klein Douwel, D.; Boonen, R. A. C. M.; Long, D. T.; Szypowska, A. A.; Räschle, M.; Walter, J. C.; Knipscheer, P. XPF-ERCC1 Acts in Unhooking DNA Interstrand Crosslinks in Cooperation with FANCD2 and FANCP/SLX4. *Mol. Cell* **2014**, *54*, 460−471.

(9) McNeil, E. M.; Melton, D. W. DNA Repair Endonuclease ERCC1-XPF as a Novel Therapeutic Target to Overcome Chemoresistance in Cancer Therapy. *Nucleic Acids Res.* **2012**, *40*, 9990−10004.

(10) McNeil, E. M.; Astell, K. R.; Ritchie, A.-M.; Shave, S.; Houston, D. R.; Bakrania, P.; Jones, H. M.; Khurana, P.; Wallace, C.; Chapman, T.; Wear, M. A.; Walkinshaw, M. D.; Saxty, B.; Melton, D. W. Inhibition of the ERCC1-XPF Structure-Specific Endonuclease to Overcome Cancer Chemoresistance. *DNA Repair* **2015**, *31*, 19−28.

(11) Fagbemi, A. F.; Orelli, B.; Schärer, O. D. Regulation of Endonuclease Activity in Human Nucleotide Excision Repair. *DNA Repair* **2011**, *10*, 722−729.

(12) Melis, J. P. M.; van Steeg, H.; Luijten, M. Oxidative DNA Damage and Nucleotide Excision Repair. *Antioxid. Redox Signaling* **2013**, *18*, 2409−2419.

(13) Zhang, J.; Walter, J. C. Mechanism and Regulation of Incisions during DNA Interstrand Cross-Link Repair. *DNA Repair* **2014**, *19*, 135−142.

(14) Porro, A.; Berti, M.; Pizzolato, J.; Bologna, S.; Kaden, S.; Saxer, A.; Ma, Y.; Nagasawa, K.; Sartori, A. A.; Jiricny, J. FAN1 Interaction with Ubiquitylated PCNA Alleviates Replication Stress and Preserves Genomic Integrity Independently of BRCA2. *Nat. Commun.* **2017**, *8*, 1073.

(15) Mason, J. M.; Das, I.; Arlt, M.; Patel, N.; Kraftson, S.; Glover, T. W.; Sekiguchi, J. M. The SNM1B/APOLLO DNA Nuclease Functions in Resolution of Replication Stress and Maintenance of Common Fragile Site Stability. *Hum. Mol. Genet.* **2013**, *22*, 4901−4913.

(16) Wyatt, H. D. M.; Laister, R. C.; Martin, S. R.; Arrowsmith, C. H.; West, S. C. The SMX DNA Repair Tri-Nuclease. *Mol. Cell* **2017**, *65*, 848−860.e11.

(17) Tacconi, E. M. C.; Badie, S.; De Gregoriis, G.; Reisländer, T.; Lai, X.; Porru, M.; Folio, C.; Moore, J.; Kopp, A.; Baguña Torres, J.; Sneddon, D.; Green, M.; Dedic, S.; Lee, J. W.; Batra, A. S.; Rueda, O. M.; Bruna, A.; Leonetti, C.; Caldas, C.; Cornelissen, B.; Brino, L.; Ryan, A.; Biroccio, A.; Tarsounas, M. Chlorambucil Targets BRCA1/2-deficient Tumours and Counteracts PARP Inhibitor Resistance. *EMBO Mol. Med.* **2019**, *11*, No. e9982.
(18) Dronkert, M. L. G.; de Wit, J.; Boeve, M.; Vasconcelos, M. L.; van Steeg, H.; Tan, T. L. R.; Hoeijmakers, J. H. H.; Kanaar, R. Disruption of Mouse SNM1 Causes Increased Sensitivity to the DNA Interstrand Cross-Linking Agent Mitomycin C. *Mol. Cell. Biol.* **2000**, *20*, 4553−4561.
(19) Wang, A. T.; Sengerová, B.; Cattell, E.; Inagawa, T.; Hartley, J. M.; Kiakos, K.; Burgess-Brown, N. A.; Swift, L. P.; Enzlin, J. H.; Schofield, C. J.; Gileadi, O.; Hartley, J. A.; McHugh, P. J. Human SNM1a and XPF-ERCC1 Collaborate to Initiate DNA Interstrand Cross-Link Repair. *Genes Dev.* **2011**, *25*, 1859−1870.
(20) Kohno, T.; Sakiyama, T.; Kunitoh, H.; Goto, K.; Nishiwaki, Y.; Saito, D.; Hirose, H.; Eguchi, T.; Yanagitani, N.; Saito, R.; Sasaki-Matsumura, R.; Mimaki, S.; Toyama, K.; Yamamoto, S.; Kuchiba, A.; Sobue, T.; Ohta, T.; Ohki, M.; Yokota, J. Association of Polymorphisms in the MTH1 Gene with Small Cell Lung Carcinoma Risk. *Carcinogenesis* **2006**, *27*, 2448−2454.
(21) Wang, X.; Wang, S.-S.; Zhou, L.; Yu, L.; Zhang, L.-M. A Network-Pathway Based Module Identification for Predicting the Prognosis of Ovarian Cancer Patients. *J. Ovarian Res.* **2016**, 73.
(22) Buzon, B.; Grainger, R.; Huang, S.; Rzadki, C.; Junop, M. S. Structure-Specific Endonuclease Activity of SNM1A Enables Processing of a DNA Interstrand Crosslink. *Nucleic Acids Res.* **2018**, *46*, 9057−9066.
(23) Sengerová, B.; Allerston, C. K.; Abu, M.; Lee, S. Y.; Hartley, J.; Kiakos, K.; Schofield, C. J.; Hartley, J. A.; Gileadi, O.; McHugh, P. J. Characterization of the Human SNM1A and SNM1B/Apollo DNA Repair Exonucleases. *J. Biol. Chem.* **2012**, *287*, 26254−26267.
(24) Ishiai, M.; Kimura, M.; Namikoshi, K.; Yamazoe, M.; Yamamoto, K.; Arakawa, H.; Agematsu, K.; Matsushita, N.; Takeda, S.; Buerstedde, J.-M.; Takata, M. DNA Cross-Link Repair Protein SNM1A Interacts with PIAS1 in Nuclear Focus Formation. *Mol. Cell. Biol.* **2004**, *24*, 10733−10741.
(25) Hazrati, A.; Ramis-Castelltort, M.; Sarkar, S.; Barber, L. J.; Schofield, C. J.; Hartley, J. A.; McHugh, P. J. Human SNM1A Suppresses the DNA Repair Defects of Yeast Pso2 Mutants. *DNA Repair* **2008**, *7*, 230−238.
(26) Doherty, W.; Dürr, E.-M.; Baddock, H. T.; Lee, S. Y.; Mchugh, P. J.; Brown, T.; Senge, M. O.; Scanlan, E. M.; Mcgouran, J. F. A Hydroxamic-Acid-Containing Nucleoside Inhibits DNA Repair Nuclease SNM1A. *Org. Biomol. Chem.* **2019**, *17*, 8094.
(27) Lee, S. Y.; Brem, J.; Pettinati, I.; Claridge, T. D. W.; Gileadi, O.; Schofield, C. J.; McHugh, P. J. Cephalosporins Inhibit Human Metallo β-Lactamase Fold DNA Repair Nucleases SNM1A and SNM1B/Apollo. *Chem. Commun.* **2016**, *52*, 6727−6730.
(28) Dürr, E.-M.; Doherty, W.; Lee, S. Y.; el-Sagheer, A. H.; Shivalingam, A.; McHugh, P. J.; Brown, T.; McGouran, J. F. Squaramide-Based 5'-Phosphate Replacements Bind to the DNA Repair Exonuclease SNM1A. *ChemistrySelect* **2018**, 12824−12829.
(29) Mangat, C. S.; Bharat, A.; Gehrke, S. S.; Brown, E. D. Rank Ordering Plate Data Facilitates Data Visualization and Normalization in High-Throughput Screening. *J. Biomol. Screening* **2014**, *19*, 1314−1320.
(30) Motegi, A.; Masutani, M.; Yoshioka, K.-I.; Bessho, T. Aberrations in DNA Repair Pathways in Cancer and Therapeutic Significances. *Semin. Cancer Biol.* **2019**, 29.
(31) O'Connor, M. J. Targeting the DNA Damage Response in Cancer. *Mol. Cell* **2015**, *60*, 547−560.
(32) Curtin, N. J. DNA Repair Dysregulation from Cancer Driver to Therapeutic Target. *Nat. Rev. Cancer* **2012**, *12*, 801−817.
(33) Kim, Y.; Spitz, G. S.; Veturi, U.; Lach, F. P.; Auerbach, A. D.; Smogorzewska, A. Regulation of Multiple DNA Repair Pathways by the Fanconi Anemia Protein SLX4. *Blood* **2013**, *121*, 54−63.
(34) Gonzalez, R. G.; Haxo, R. S.; Schleich, T. Mechanism of Action of Polymeric Aurintricarboxylic Acid, a Potent Inhibitor of Protein-Nucleic Acid Interactions. *Biochemistry* **1980**, *19*, 4299−4303.
(35) Xu, Z. Mechanics of Metal-Catecholate Complexes: The Roles of Coordination State and Metal Types. *Sci. Rep.* **2013**, *3*, 2914.

https://doi.org/10.1021/acsomega.0c03528
ACS Omega 2021, 6, 9352−9361